

## Moho depth and sediment thickness estimation beneath the Red Sea derived from satellite and terrestrial gravity data

Ahmed Salem<sup>1</sup>, Chris Green<sup>2</sup>, Simon Campbell<sup>3</sup>, J. Derek Fairhead<sup>2</sup>,  
Lorenzo Cascone<sup>3</sup>, and Lee Moorhead<sup>3</sup>

### ABSTRACT

We sought to map the depth and density contrast of the Mohorovičić discontinuity (Moho) across the Red Sea area and to model sedimentary thickness from gravity data. The gravity data that are used are a combination of satellite and terrestrial gravity data processed into a Bouguer anomaly grid. A 200-km low-pass filter was used to separate this grid into regional and residual gravity grids. We inverted the regional gravity grid to a Moho depth map based on a density contrast map that is constrained by published seismic results. The interpreted Moho is shallowest (<10 km) along the axis of the central Red Sea, ~13 km along the axis to the south, and ~20 km in the northern Red Sea. The depth increased to ~20–25 km at the coast and 35–40 km in the adjacent continents. The residual

gravity data provided insights into the tectonic fabric along the whole rift and provided a good correlation with magnetic lineaments where these are available. We used the complete Bouguer anomaly to model sedimentary thicknesses constrained by wells and the interpreted Moho. The modeling results are consistent with the presence of large-scale, ridge parallel tilted fault blocks forming subbasins with a maximum depth of about 6–7 km. Our models suggest that the northern Red Sea has an asymmetric basement surface with the western side deeper than the eastern side. The results indicate the presence of oceanic crust in the central and southern parts of the Red Sea, but not in the north. The very thin crust and interpreted oceanic crustal density in the central Red Sea suggest that this area is fully oceanic — although possibly quite young.

### INTRODUCTION

The Red Sea is considered to be an embryonic ocean and is a good example of an active continental rift that is in its early stages of continental break-up. The rifting in the region was initiated around 30 Ma (Bosworth and Burke, 2005) with the movement of the Arabian plate to the northeast away from the Nubian (African) plate to the southwest. Sea-floor spreading in the southern part of the area started between 9 and 12 Ma (Makris et al., 1991) and 5 Ma (Roeser, 1975; Bosworth and Burke, 2005).

Many models have been proposed for the evolution of the Red Sea, ranging from purely active (magmatically driven) to purely passive (mechanically driven) rifting (e.g., Ghebreab, 1998; Bosworth and Burke, 2005). One major point of controversy is the extent of oceanic crust within the Red Sea. Some authors (e.g., Avedik

et al., 1988; Gaulier et al., 1988) interpret oceanic crust along the axis of most of the Red Sea based on seismic velocities. This is consistent with the recent model proposed by Bosworth and Burke (2005) (Figure 1). Others (e.g., Cochran and Martinez, 1988; Egloff et al., 1991) consider that oceanic crust is much more restricted and explain the seismic velocity data in other ways.

In many instances, the debate on crustal structure is informed by the availability and use of seismic reflection/refraction data that image features down to and into the upper mantle. However, the major salt deposition stage in the evolution of the Red Sea restricts the imaging capability of seismic reflection data over much of the area. Thus, the subsalt section (i.e., presalt sediments, basement and crustal rocks including the Mohorovičić discontinuity [Moho]) is poorly mapped.

The aim of this study is to further inform the debate on the tectonic evolution of the Red Sea region by using gravity data to

Manuscript received by the Editor 27 April 2012; revised manuscript received 22 May 2013; published online 6 September 2013.

<sup>1</sup>Getech, Leeds, UK; University of Leeds, Leeds, UK, and Nuclear Materials Authority, Cairo, Egypt. E-mail: ahmedsalem30@yahoo.com.

<sup>2</sup>Getech, Leeds, UK and University of Leeds, Leeds, UK. E-mail: chris.green@getech.com; derek.fairhead@getech.com.

<sup>3</sup>Getech, Leeds, UK. E-mail: simon.campbell@getech.com; lorenzo.cascone@repsol.com; lee.moorhead@getech.com.

© 2013 Society of Exploration Geophysicists. All rights reserved.

interpret the deep structure that is hard to resolve with the available seismic reflection and seismic refraction data alone. Our specific objectives are to map the depth and density contrast of the Moho across the study area and subsequently forward-model the sedimentary thickness in the southern, central and northern Red Sea more reliably. The results could then be interpreted in terms of the extent of oceanic crust in the region.

## WORK FLOW

At the margins of oceans and especially in young ocean basins, crustal stretching and direct heating effects from upwelling hot mantle will generate thermal anomalies in the upper mantle and crust. These will lead to density variations, especially in the uppermost mantle. The generation of new higher-density oceanic crust

will further alter the density contrast across the Moho. These density variations have been included in previous gravity models across the Red Sea. For example, Makris et al. (1991) express this density variation as large blocks of lower density mantle below the rift. Predictive thermal models of the lithosphere due to rifted sedimentary basins have been devised by McKenzie (1978) and these have been incorporated into iterative gravity inversion strategies by Chappell and Kusznir (2008) using smoothly varying upper mantle densities that depend on the degree of stretching of continental crust and the age of oceanic crust. In this study, however, we have chosen to model the effective density variation based on seismic control points combined with the gravity data themselves.

Figure 2 shows a flowchart that outlines how we derive the Moho model and representative 2D models so that we can better understand the tectonic evolution of the Red Sea region. We do not use the constraints provided by a specific model of thermal processes in new oceanic rifts. Instead, we compile a gravity data set and apply careful separation of the gravity field into regional and residual components. We then use the regional component to generate a model of Moho depth and the variation in the Moho density contrast over the Red Sea area. This provides information about the nature of the crust and upper mantle along the Red Sea. We then examine the residual component which provides further insights into the tectonic fabric of the area, as well as information on the Red Sea sedimentary basins, including the presalt section.

## CONTROL ON CRUSTAL THICKNESS IN THE RED SEA REGION

To achieve the objectives of the present study, we needed to use independent data to constrain the Moho depths in parts of the area. Since the early 1960s, many wide-angle seismic surveys have been conducted in the Red Sea, the Afar depression, and the western Arabian Shield with the aim of understanding the deep geology of the area and determining the crustal and uppermost-mantle structure of the major units of the Afro-Arabian rift system. Depths to Moho are included *inter alia* in many of the resulting publications. These are based on different interpretation methodologies and conceptual geologic models. Some of these studies also modeled gravity data.

Seismic refraction data, due to their wide-angle raypaths and inherent low frequencies, are not as restricted by near-surface salt as seismic reflection data. However, there is still the potential for inconsistencies in their interpretation based on different physical and conceptual models. Because of this, and due to the large number of individual seismic lines, the Moho seismic control for this study (Figure 3) has been drawn from two wide-ranging reviews of available

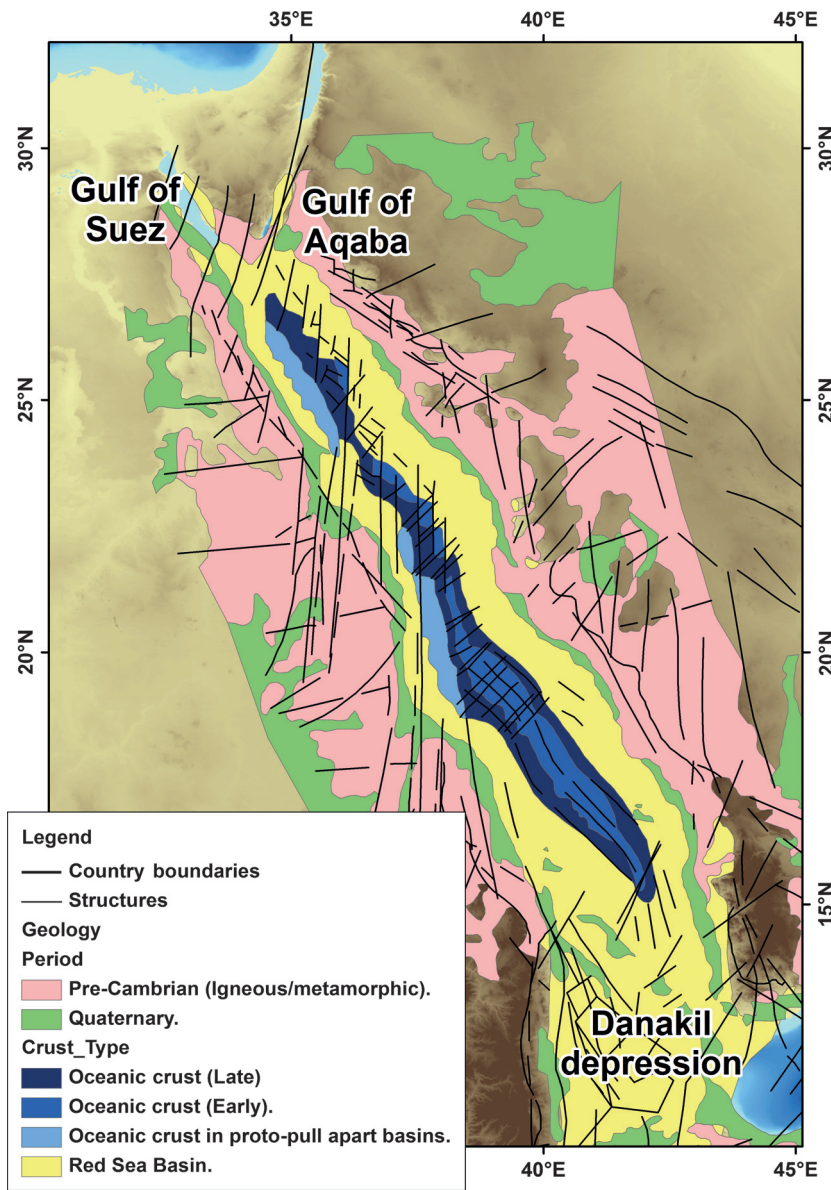


Figure 1. Present-day tectonic elements map of the Red Sea region (after Bosworth and Burke, 2005). This interpretation shows the maximum amount of oceanic crust — extending almost the full length of the Red Sea.

seismic refraction data (Prodehl and Mechle, 1991; Prodehl et al., 1997). These have been supplemented by a more recent receiver function study by Hansen et al. (2007) that sampled Moho depths at different points — mostly on the Arabian side. Although compilations of Moho depth in Africa have been produced (e.g., Seber et al., 2001), good controls on Moho depth on the African side of the Red Sea are limited. Moho depths over the area are seen to vary widely from 40 km in the Arabian Shield and ~35 km in Africa to ~20 km along the shoreline and 8–14 km along the axis of the Red Sea. The shallowest Moho depths (8–14 km) are mapped in the central section of the Red Sea area with the Moho slightly deeper (11.5–15 km) in the north.

The Red Sea rift system is interpreted to be underlain by material with anomalous mantle P-wave ( $P_n$ ) velocities of less than  $8.0 \text{ km.s}^{-1}$ , whereas along the rift flanks, the mantle  $P_n$  velocity is greater than or equal to  $8.0 \text{ km.s}^{-1}$  (Prodehl et al., 1997). Figure 4 shows a profile of uppermost mantle seismic velocity across the Red Sea based on results published by Egloff et al. (1991). Generally, the seismic velocities of the uppermost mantle decrease from the rift shoulder to the central ridge axis. Although the distribution of Moho control points shown in Figure 3 contains significant gaps, use of these points as control for the gravity inversion will allow an improved Moho map to be generated.

## GRAVITY DATA

Figure 5 summarizes the process that we use to integrate satellite gravity with terrestrial gravity, topography, and bathymetry data sets to generate a combined Bouguer anomaly grid (Figure 6a). Figure 6b shows the coverage of the different gravity data sets. This gravity data set is a combination of GETECH's Trident satellite data (Fairhead et al., 2009) offshore with gridded data from compiled gravity point data and EGM2008 (Pavlis et al., 2012) in adjacent land areas. The Bouguer reduction density of  $2670 \text{ kg.m}^{-3}$  that is used throughout represents a typical value for basement rocks.

The Trident data set is a stack or average of the best three available satellite altimeter gravity solutions. The three solutions used are Sandwell and Smith v16.1, Danish National Space Center (DNSC08), and GETECH satellite solution (for details, see Fairhead et al., 2009). The  $0.02^\circ$  free-air anomaly grid has half-wavelength resolution of 6.5 km and an accuracy of approximately 2 mGal (rms discrepancy), based on correlations with higher-resolution marine gravity surveys (Fairhead et al., 2009).

Onshore Africa, the  $5' \times 5'$  grid of simple Bouguer anomaly from GETECH's African Gravity Project (AGP) is used. This is a compilation of Bouguer anomaly point data on and offshore Africa (Green and Fairhead, 1996).

EGM2008 is a global gravity model compiled from a range of sources including land, marine, and airborne measurements and satellite altimetry over the oceans. GRACE satellite data are used to define the long wavelengths (Pavlis et al., 2012). The limiting resolution of EGM2008 is  $5' \times 5'$ , but the actual resolution is often worse locally, depending on the coverage and resolu-

tion of the available terrestrial gravity data. Onshore Arabia, the EGM2008 free air anomaly is low-pass filtered at  $0.3^\circ$  to remove obvious artifacts.

An integrated topography/bathymetry grid is generated by merging shuttle radar topography mission (SRTM) data onshore with regridded ship sounding bathymetry data. This grid is used to calculate Bouguer and terrain corrections for offshore areas and Bouguer corrections for Arabia. Terrain corrections are calculated in the space domain out to a radius of 166.7 km, using the line mass formula with earth curvature taken into account. All the corrections are filtered to match the resolution of the Trident or EGM2008 data before applying them to generate Bouguer anomaly grids.

The three land and marine Bouguer anomaly grids are joined by blanking narrow areas of relatively poor satellite data close to the coast and smoothly filling the resulting gaps to give a continuous Bouguer anomaly grid. Visual inspection of the satellite data set reveals the presence of occasional mismatches or smooth areas close to the coast, especially around reefs and islands. This suggests that the coastal strip is probably the least well-defined area, although this satellite grid does have much more continuous and reliable coverage than would be achieved with available shipborne data. The data resolution is roughly compatible with most of the onshore coastal area, but there are also some larger data gaps further inland.

## SEPARATION OF GRAVITY ANOMALIES

The resulting Bouguer anomaly (Figure 6a) contains all of the gravity effects stemming from lateral density variations within the earth. To simplify the model and the modeling process, the Bouguer anomaly may be considered principally as the sum of the gravity contributions of a series of layers or geologic units within the crust and upper mantle. For the Red Sea region, we

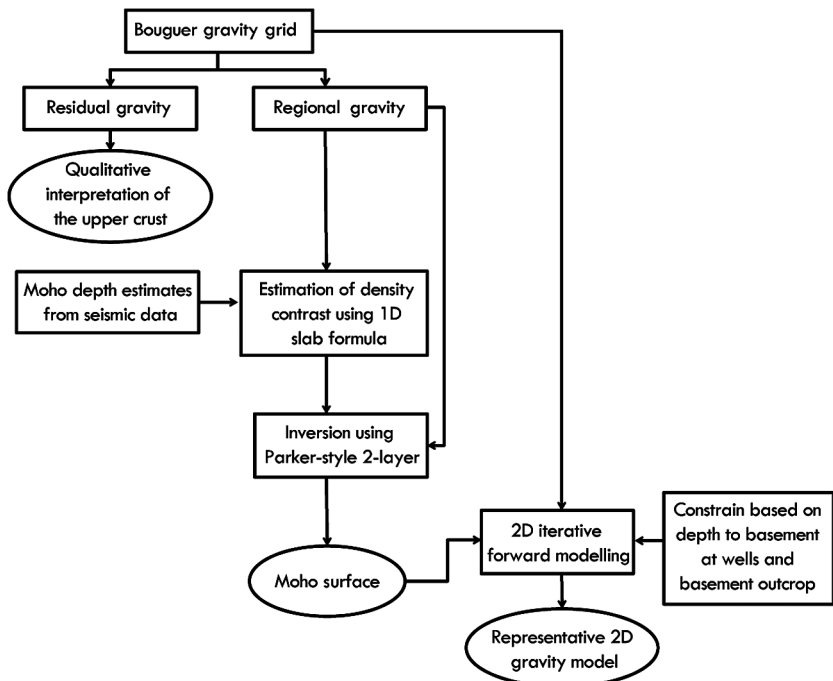


Figure 2. Flowchart of the modeling process used in this study, identifying source data, intermediate, and final outputs.

consider the gravity anomaly to be primarily produced by local variations in the thickness and/or densities of the following units:

- 1) Sea water (density  $\rho$  and depth are known and incorporated in the Bouguer anomaly, so there is no effect when using Bouguer anomaly data)
  - 2) Postsalt sediments ( $\rho$  is a function of depth that can be estimated based on seismic velocity and well data)
  - 3) Salt ( $\rho$  is generally known locally from well data and depths-to-top are well imaged from seismic data; depth-to-base-salt may also be imaged from seismic data, but this is less well known)
  - 4) Presalt sediments ( $\rho$  and thickness are generally unknown)
  - 5) Upper mantle (i.e., a shallow Moho or crustal thinning under the rift will cause a positive gravity effect) (spatial variation of  $\rho$  and depth to the mantle [Moho] are generally unknown except in isolated locations where seismic refraction studies have been carried out).

Several of these gravity contributions would be expected to have a similar shape — elongate anomalies parallel to the Red Sea. The gravity anomaly associated with a reduction in the depth to the Moho (“Moho gravity anomaly”) (i.e., a lateral increase in the thickness of the upper mantle) is identified as the dominant pos-

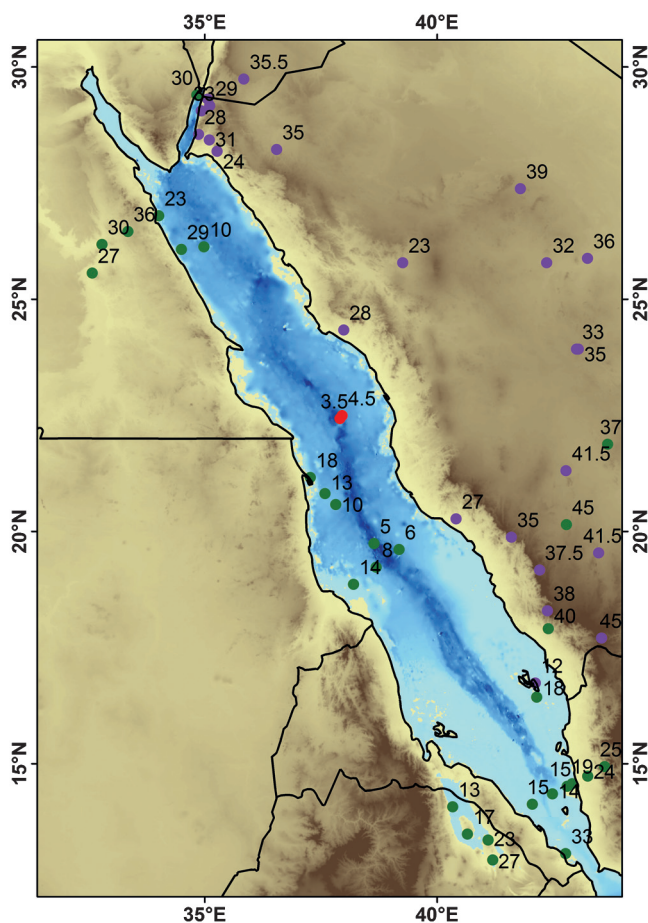


Figure 3. Point depths to Moho (km) based on values taken from published depths from interpretation of seismic data overlaid on terrain and bathymetry — Hansen et al. (2007) (purple points); Prodehl and Mechle (1991) (red point); Prodehl et al. (1997) (green points).

itive gravity contribution in the system. Our aim is to separate this gravity anomaly and interpret it in terms of a variable Moho depth and density contrast model. Removal of this contribution should then assist in isolating the gravity response associated with the sediments. Knowledge of the upper section would allow an improved definition of the important presalt sedimentary section.

There have been many different approaches used for this problem of separating the contribution due to Moho depth variations and upper crustal composition, generally involving subtracting a long-wavelength trend from the data in either space or frequency domains. This assumes that Moho and upper mantle contributions have a longer wavelength than those from the upper crust, so this separation is often referred to as a “regional-residual” separation. The availability of control data and a good conceptual model are important for a robust, reliable regional-residual separation. The regional-residual separation approach for isolating contributions from Moho depth variations and upper-crust sources is questionable in this instance because both sources produce anomalies that have widths similar to that of the Red Sea. However, we will assume that the two may still be separable because the Moho gravity anomaly will generally be broader due to its greater depth.

Working with the merged gravity data grid, we applied low-pass filters with a range of different cut-off wavelengths. Figure 7a, 7b, and 7c shows low-pass filtered gravity grids using 100, 200, and 300-km cut-off wavelengths (Butterworth order 4). The results are assessed in terms of the match of regional and residual components to the expected signal due to known geology such as Moho depth generally decreasing from the continents toward the central axis of the Red Sea (see Figures 3 and 4). The 100-km regional (Figure 7a) contains short-wavelength signal (e.g., along the Arabian coast) incompatible with this simple model, whereas the 300-km regional (Figure 7c) is too smooth to fit the expected shapes of the contributions from the depth variations of the Moho across the rift. The 200-km regional (Figure 7b) appears to contain wavelengths suitable for fitting with Moho depth variation, which is indeed found to be the case in the subsequent inversion.

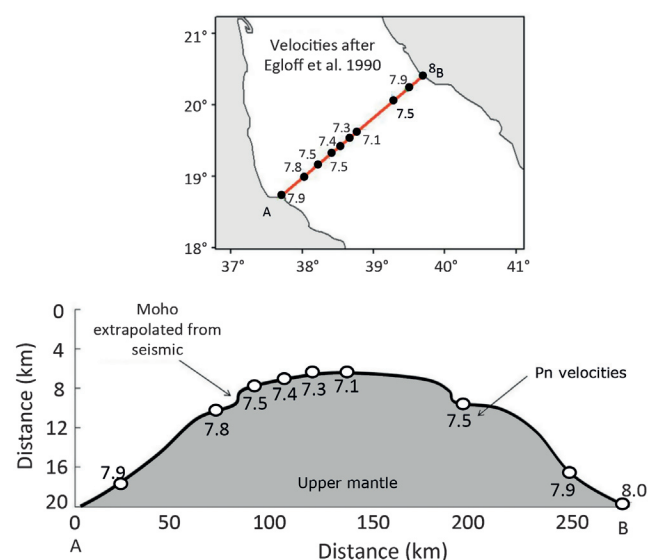


Figure 4. Example of refracted, upper mantle P-wave velocity ( $Pn$ ) (km/s) and depth variation across the Red Sea — (after Egloff et al., 1991).

The corresponding residual anomaly (Figure 8) also fits with known and anticipated geologic features, i.e., elongate negative anomalies either side of the central ridge corresponding with elongate sedimentary basins.

## MAPPING THE MOHO SURFACE

To model the 3D geometry of the Moho interface for the Red Sea area, we apply a 3D iterative inversion to the regional gravity grid. We use Geosoft's GM-SYS 3D software, which is based on the method of Parker (1973). We used a two-layer model with variable density contrast. Constraints for the depth and the density contrast are based on a review of published depths to Moho in the Red Sea and surrounding areas (Figure 3). We estimate Moho density contrast values ( $\Delta\rho$ ) at each control point based on seismic Moho depth and Bouguer anomaly ( $\Delta g$ ) values using a simple 1D slab formula  $\Delta\rho = \Delta g / 2\pi G \Delta h$  where  $G$  is the gravitational constant and  $(\Delta h)$  is the vertical thickness interval between the seismic Moho and a reference depth of 50 km below sea level. This value of 50 km is the effective base of our model and the assumption that we made is that all upper mantle density variations are shallower than this level. Derived density contrasts therefore largely relate to density variations within this uppermost part of the mantle. A similar assumption to this is inherent in Makris et al. (1991).

Due to the sparse and uneven distribution of the seismic control, a rationale is required for extending the density contrast points over the whole area. The calculated density contrast values are manually smoothed such that they are symmetric about the axis of the Red Sea (Figure 9). Resulting density contrasts along the middle of the Red Sea are very small ( $200 \text{ kg.m}^{-3}$ ), but increase to  $500 \text{ kg.m}^{-3}$  in stable continental areas. This apparent uppermost mantle density reduction in the Red Sea is consistent with the observed reduced seismic (Pn) velocities (Figure 4) and suggests a variation in the composition and/or temperature of the mantle across the area. This could be related to local high-temperature material in the upper mantle, which would be consistent with the substantially higher heat flow in the Red Sea compared to adjacent continental areas (Cochran et al., 1986). It is likely that the observed density contrast is enhanced by an increase in density of the crust toward the middle of the Red Sea in areas where oceanic crust has developed.

Figure 10 shows the depth to Moho surface relative to sea level from the 3D inversion. Generally, the inverted Moho surface is around 20–25 km deep in the coastal areas, becoming deeper to 35–40 km on the continents, and becoming shallower to 10–15 km along the axis of the Red Sea. The shallowest Moho is less than 10 km deep in the central Red Sea. In the northern part of the Red Sea, the depth to Moho is between 10 and 13 km along the axis and 20 km close to the coastline. Prutkin and Saleh (2009) obtain similar results from inversion of marine gravity data in the northern Red Sea. Avedik et al. (1988) and Gaulier et al. (1988) estimate the depth to Moho as 11.5–15 km at  $25^\circ$  north. These depths are generally in good agreement with our results, although

the 200-km low-pass filter used in this study may limit the inverted depths, such that, especially in the narrow rifts of the Gulfs of Suez and Aqaba, the Moho is probably shallower than the inversion results indicate. In the southern area, the depth to Moho is even shallower — 9.8 km at latitude  $20^\circ$ . This is consistent with seismic refraction results (Prodehl, 1985) that show the Moho at a depth of about 40 km beneath Saudi Arabia thinning to 8–14 km depth in the southern Red Sea. Figure 11 shows the comparison of the Moho depths from the inversion with the depths from the control data. The correlation is generally good, indicating that the constraint data are being honored by the inversion. However, the match is not perfect, despite the control data being incorporated in the process. This is probably because the density model has been smoothed to avoid unconstrained rapid changes and because the inversion is 3D whereas, the control has been applied in 1D. The positive bias in the inverted depth values (i.e., the inverted depths being deeper in shallow areas) could be a consequence of the regional Bouguer anomaly being too smooth to image the shallow and complex structure of the Moho beneath the oceanic crust close to the ridge axis.

Gravity and seismic Moho depths suggest that the thinnest part of the crust is located in the central area of the Red Sea rift ( $\sim 20^\circ \text{ N}$  — see Figure 10). Moreover, the Moho density contrast is seen to be smallest in this area, suggesting not only lower density, hot upper mantle as also implied by the velocity data in Figure 4, but also that the crust is higher density and therefore likely to be oceanic in nature.

## QUALITATIVE INTERPRETATION OF THE RESIDUAL GRAVITY ANOMALIES

Figure 12 shows a qualitative interpretation of the residual Bouguer gravity in the Red Sea Basin. The various narrow positive

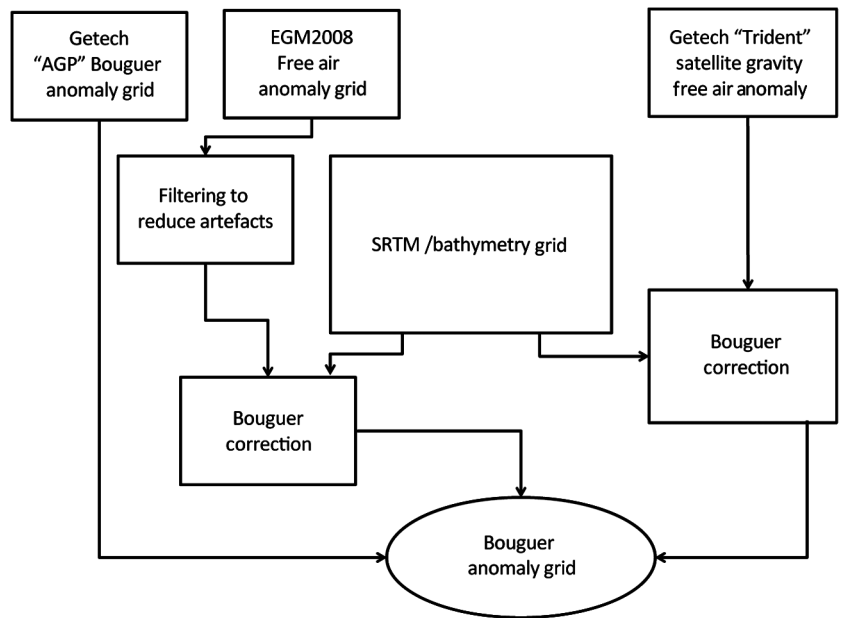


Figure 5. Flowchart to describe the generation of the gravity data set used in this study. AGP (Green and Fairhead, 1996) is a compilation of Bouguer anomaly land and marine data for Africa; EGM2008 (Pavlis et al., 2012) is a global free-air-anomaly grid incorporating a range of terrestrial and satellite gravity data sets; Trident (Fairhead et al., 2009) is a satellite free-air-anomaly grid generated from previous satellite gravity models.

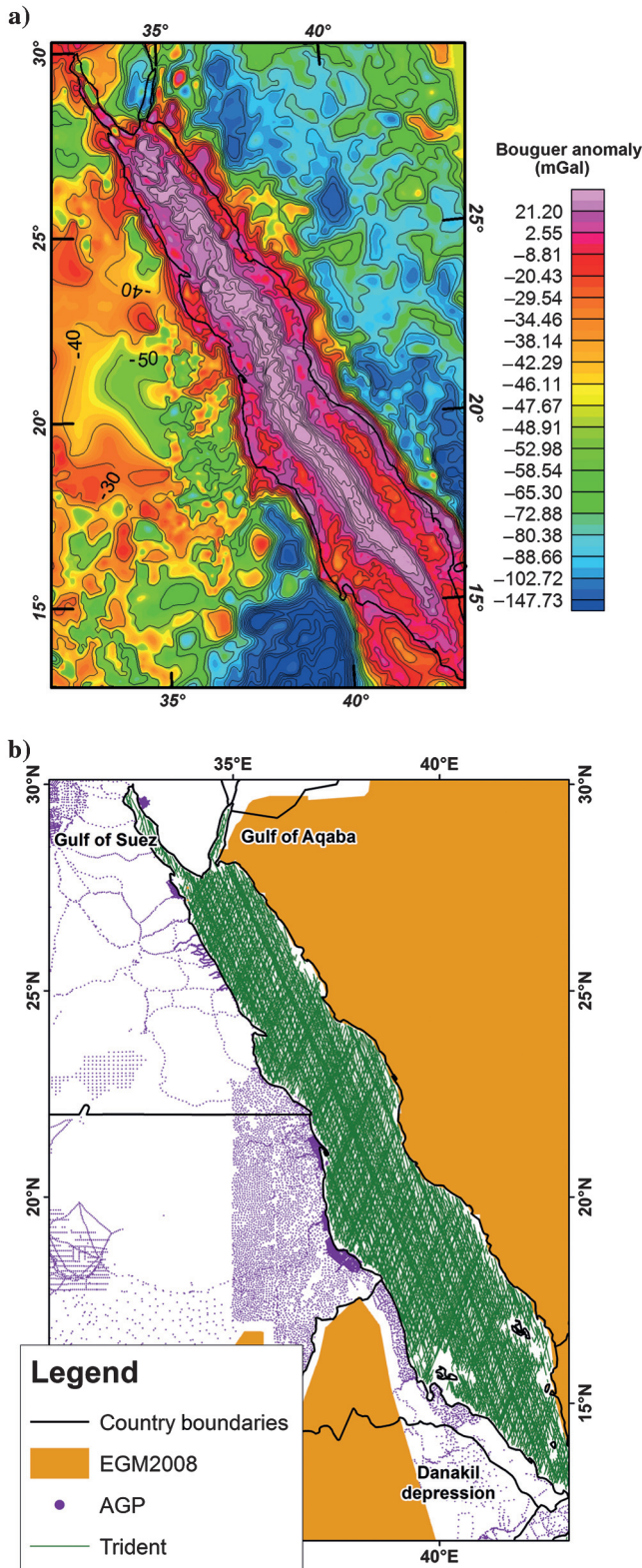


Figure 6. (a) Bouguer anomaly ( $\text{density } 2670 \text{ kg} \cdot \text{m}^{-3}$ ) of the Red Sea — based on the data sets in (b). (b) Gravity data coverage in the Red Sea region. Note that EGM2008 is only available as an  $\sim 9\text{-km}$  gravity grid. Satellite tracks indicate the extent of coverage only; these gravity data are only available on an  $\sim 2\text{ km}$  grid.

and negative anomalies, which are now readily visible, demonstrate that the residual grid is a much better tool for qualitative interpretation of shallower features than the Bouguer anomaly itself. Such narrow anomalies must be relatively shallow and hence, mostly related to features in the upper crust. These features have tectonic significance that helps in understanding the history and geologic structure of the Red Sea.

For the southern Red Sea ( $15^\circ\text{N}$  to  $20.5^\circ\text{N}$ ), the residual gravity is characterized by a continuous, sinuous gravity high with a narrow central low along the axial zone of the Red Sea. This is interpreted as the response related to high-density ocean crust formed within the last 5 Ma (Cochran and Karner, 2007), the axial low representing the active ocean rift. The axial high is flanked on both sides by negative anomalies reflecting the sedimentary cover over what has been interpreted as extended continental crust by Richter et al. (1991) based on the interpretation of the existence of pre-Miocene sedimentary rocks from seismic data. The crust to either side of the central zone is interpreted as stretched continental crust covered by thick sedimentary sequences. This section of the Red Sea represents the early or embryonic stage of an oceanic basin.

Figure 13 shows the EMAG-2 total magnetic field map of the Red Sea Basin. EMAG-2 (Maus et al., 2009) is a global compilation of airborne, marine, and satellite magnetic measurements presented as a  $2' \times 2'$  grid. The crust in the axial portion in the southern Red Sea may be of oceanic type, because it is associated with linear magnetic anomalies (Allan, 1970; Phillips, 1970) and seismicity (Fairhead and Girdler, 1970). Fault-plane solutions determined by Fairhead and Girdler (1970) show strike slip mechanisms consistent with the opening of the Red Sea, with strike azimuth between  $49^\circ$  and  $53^\circ$  (Figure 12). The lack of any axial zone offsets suggests that the relative opening of the Nubian and Arabian plates has been more or less perpendicular to the axial trend and of similar strike to the focal mechanisms. At the southern end of the Red Sea (south of  $15^\circ\text{N}$ ), the axial zone becomes less pronounced due to the axis of spreading sidestepping to the west into the Danakil Depression of Afar, Ethiopia. This structural offset is clearly seen in the seismicity (Figure 14) and magmatism (Bastow and Keir, 2011).

Within the central Red Sea ( $20.5^\circ\text{N}$  to  $23^\circ\text{N}$ ), the axial gravity high is subdivided into two distinct blocks by three northeast-southwest-trending structures previously called “intertrough zones” by Izzeldin (1987). These three northeast-southwest zones are considered to represent a set of dextral transforms with strike direction of  $\sim 40^\circ$  progressively offsetting the axial zone to the northeast from south to north. Seismicity as reported by the International Seismological Centre (ISC) is absent, suggesting that the stress is low and is being taken up by microseismicity and creep processes.

In the northern Red Sea (north of  $23^\circ\text{N}$ ), the residual anomaly is spatially complex, including shorter wavelength anomalies associated with the marginal sedimentary basins, magmatic intrusions, and narrow linear zones that could represent thinned continental crust or rotated crustal block faulting. The axial zone that is found further south is absent in the north, and seismicity is restricted to the northernmost area, close to the Gulfs of Suez and Aqaba, where a scatter of  $M_w < 5.0$  events occur (Figure 14). The view of Cochran and Karner (2007), supported here, is that the northern Red Sea is underlain by extended continental crust which has not yet fully split apart to generate oceanic crust, possibly due to its slow spreading rate (around  $12 \text{ mm/year}$  — ArRajehi et al., 2010). The residual gravity map (Figure 8) helps to visualize the spatial geometry of the

structures that control the evolution of the northern Red Sea. For example, several distinct northeast to north-northeast-trending gravity highs can be identified and these appear to be associated with magnetic lineaments linking volcanic centers (marked in Figure 12). Although there is not a one-to-one correlation between the gravity and magnetic lineaments, their directions are by and

large close to small circles around the generally accepted Euler pole between Nubia and Arabia ( $\sim 20^\circ\text{E}$ ,  $31^\circ\text{N}$ ; ArRajehi et al., 2010). Hot brine deeps and volcanoes (Figure 12) in the northern Red Sea reflect areas of very high geothermal heat flow. The Conrad, Ocean, and Shaban Hot Brine Deep are closely associated with strong dipole anomalies (Ehrhardt et al., 2005), which lie on

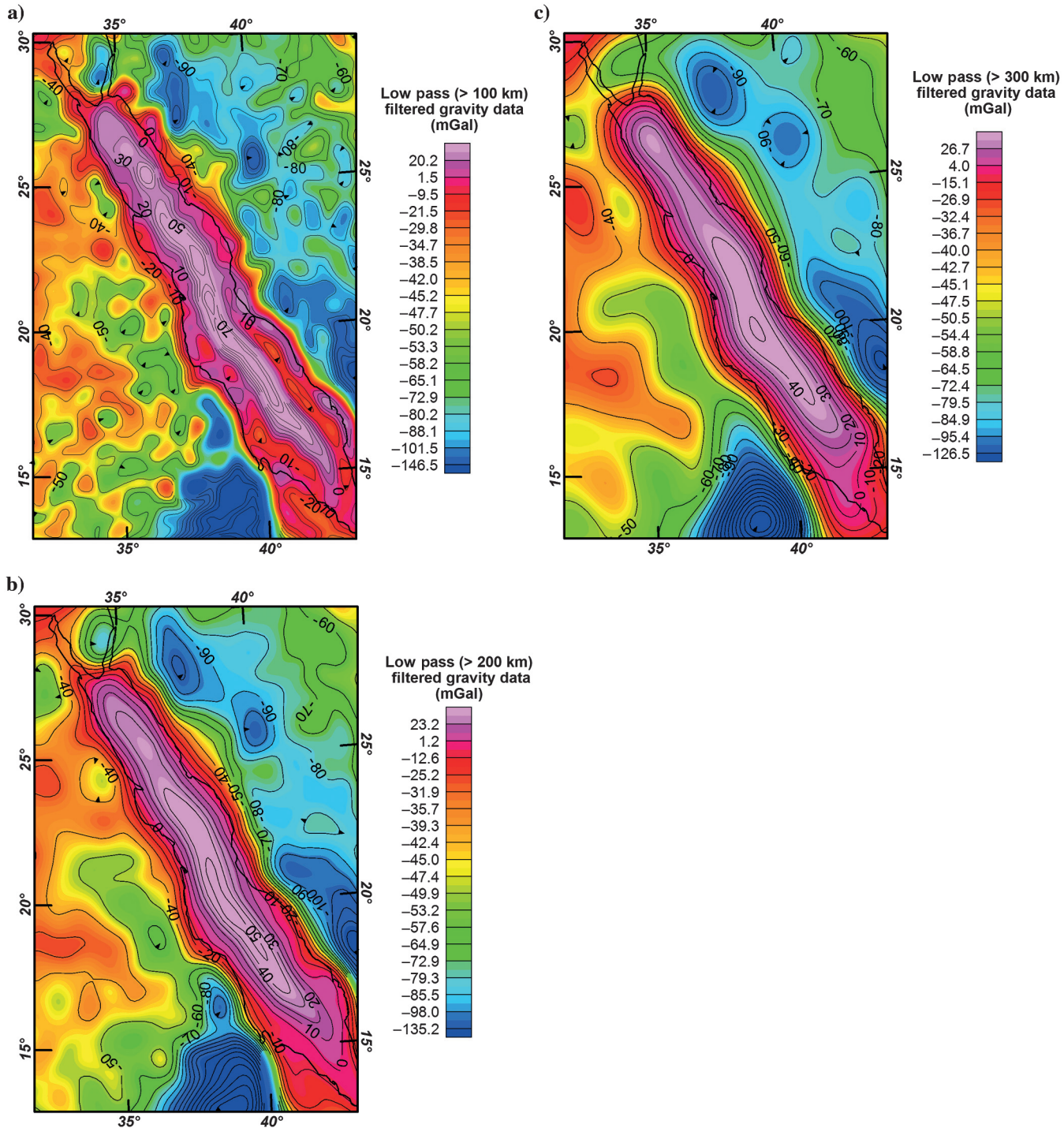


Figure 7. (a) Low-pass ( $>100$  km) filtered gravity data of the merged satellite and onshore gravity data of the Red Sea region. (b) Low-pass ( $>200$  km) filtered gravity data of the merged satellite and onshore gravity data of the Red Sea region. (c) Low-pass ( $>300$  km) filtered gravity data of the merged satellite and onshore gravity data of the Red Sea region.

magnetic lineaments marked on Figure 12. Thus, these lineaments could be embryonic sites of oceanic transforms where magmatic bodies have intruded the basement to a high level (i.e., shallower than the Curie isotherm depth).

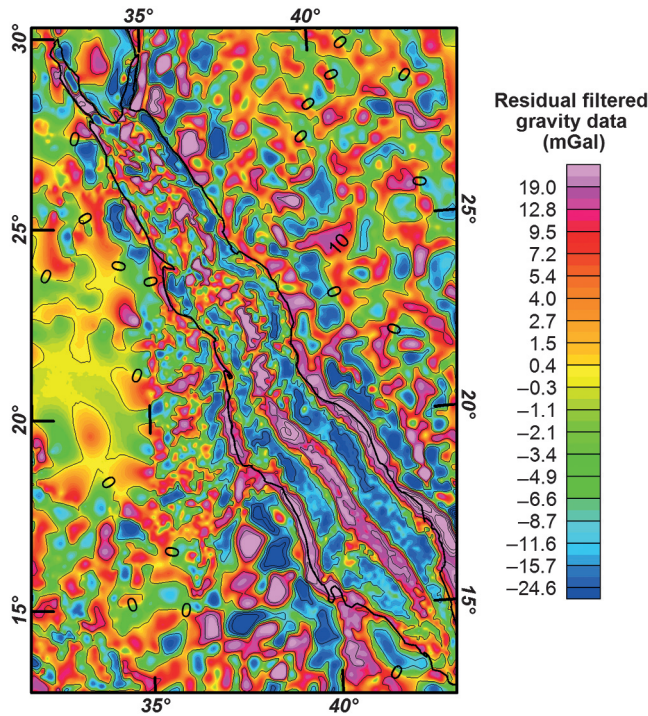


Figure 8. Residual filtered gravity data of the merged satellite and onshore gravity data of the Red Sea region after removal of long wavelength components of the signal defined by a low-pass filter ( $>200$  km).

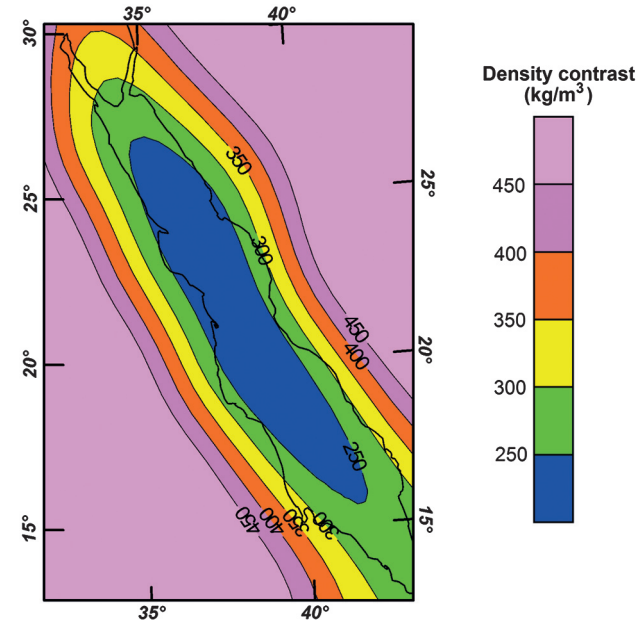


Figure 9. Moho interface density contrast model.

Linear residual gravity highs flank the sides of the axial bathymetric low in the northern Red Sea, but have much lower amplitude than in the central and southern Red Sea. They do not have any distinct magnetic expressions (Ehrhardt et al., 2005). This suggests that they may represent more localized Moho thinning zones located below the Curie isotherm depth or that they are associated

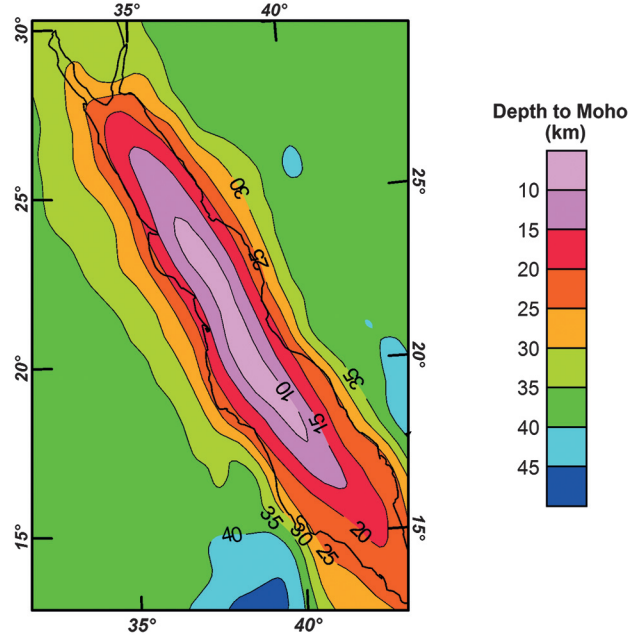


Figure 10. The topography of the Moho interface from 3D inversion of the filtered gravity data.

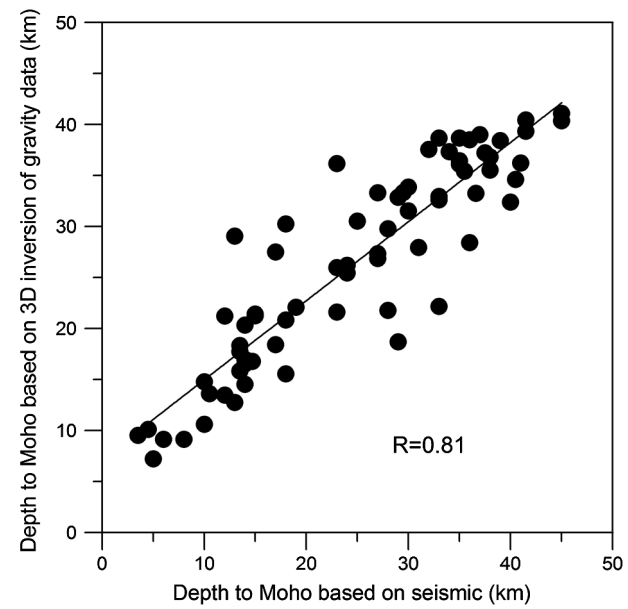


Figure 11. Comparison of depths to Moho interface based on interpretation of seismic refraction data and results of 3D inversion of gravity data. The generally good correlation suggests that the whole process (regional-residual separation, density estimation, and inversion) has been well controlled, although a bias at shallow depths is noted.

with rotated basement fault blocks. The only direct evidence of basement structures directly influencing the Red Sea structures is the Najd fault system at the northern end of the Red Sea. This northwest-trending fault zone is plotted in Figure 12 and can be traced into the Red Sea. Similar trends can be identified elsewhere in the gravity field of the northern Red Sea, but have not been delineated in Figure 12.

There are four clear implications of the interpretations arising from this qualitative study on our 2D modeling. (1) Apart from the clear negative sedimentary anomalies parallel to the coastlines of the Red Sea, much of the axial region of the Red Sea is either oceanic crust (central and southern Red Sea) or a complex set of magmatic bodies and/or rotated basement fault blocks (northern Red Sea). (2) The Red Sea opening is more or less consistent with conventional rigid plate Nubia-Arabia rotation. (3) Observed transforms or prototransforms identified through their gravity/magnetic expression lie close to small circles and will generate relatively little stress. These inferred transforms divide the Red Sea into segments where parallel crustal thinning zones are occurring along the flanks of the bathymetric low. (4) Local magmatic intrusions in the north

provide enhanced heat flow, which may mark the early stages of an oceanic system in this area.

## REPRESENTATIVE 2D GRAVITY MODELS

We have carried out iterative 2D forward modeling over three profiles: A-A' in the north, B-B' in the center, and C-C' and in the southern Red Sea (see Figure 12 for locations). For these models, we use the complete Bouguer anomaly data and include the deep geology previously interpreted from the regional gravity field. In this way, we can test that the Moho and upper mantle model fits within a coherent and complete gravity model and also illustrate how sedimentary geology can be interpreted from the gravity data. We rely on information from six basement wells published by [Beydoun and Sikander \(1992\)](#) to constrain the interface between sedimentary cover and basement. The models are also constrained by basement outcrop (Figure 1) at the ends of the three profiles. The Moho depths and upper mantle densities are taken directly from the inversions described above.

For the purpose of modeling, a simple sedimentary layer with density  $2400 \text{ kg.m}^{-3}$ , upper crust with density  $2800 \text{ kg.m}^{-3}$  and lower crust with density  $2900 \text{ kg.m}^{-3}$  are used. These densities

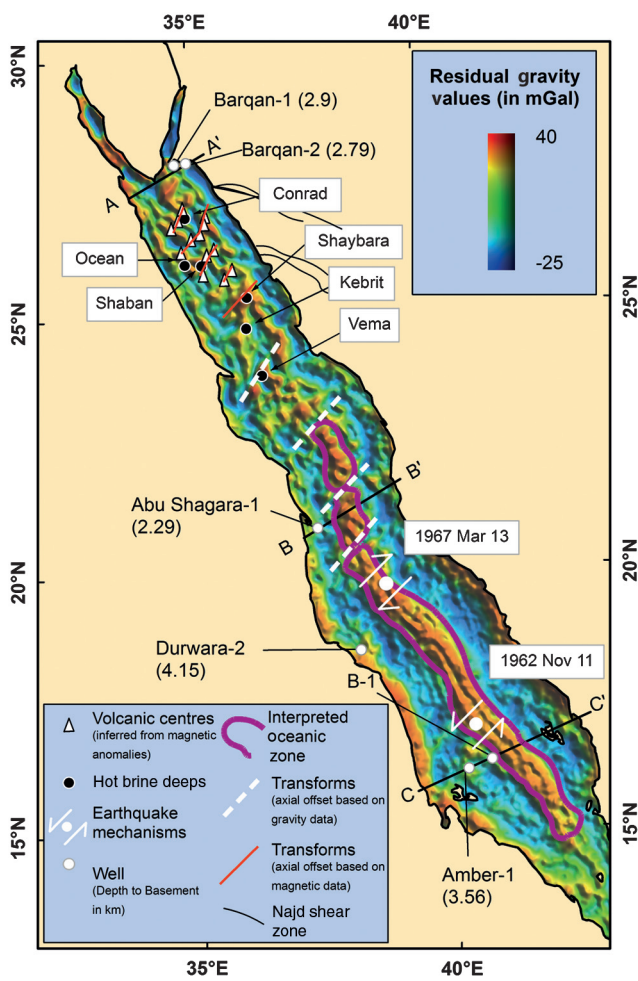


Figure 12. Interpreted residual gravity of the Red Sea basin, showing location of hot brine deeps, volcanoes (after [Cochran and Karner, 2007](#)), earthquake mechanisms, and proposed transforms. Northwest-southeast trending faults of the Najd fault zone are shown as black lines onshore at the northeastern end of the Red Sea.

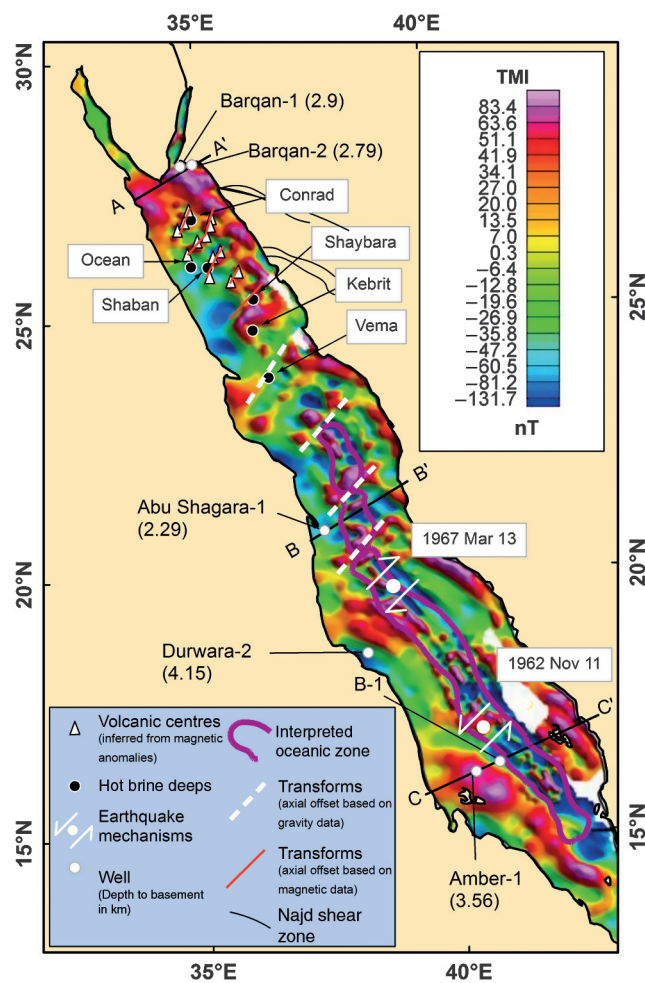


Figure 13. Total magnetic intensity map of the Red Sea ([Maus et al., 2009](#)). The features in the overlay are the same as those shown in Figure 12.

are typical of the range of values found by Makris et al. (1991) in their 2D gravity and seismic models. These densities are subject to uncertainty, so we could have used other values. We expect that the use of different densities for the sediments and/or basement would have changed the depths of the interpreted basins, but would not have significantly altered their shape. Lateral density variations, such as those generated by localized salt features, would also subtly alter the general shape of interpreted basins without altering the significant outcomes of the modeling work.

Figure 15a shows the northern Red Sea model along A-A'. It is inferred from the qualitative interpretation of the residual gravity data that oceanic crust is absent from this area, and hence, the 2D model is interpreted with predominantly stretched continental crust. Sediment thickness toward the eastern side is partially constrained by well data. This means that, to successfully model

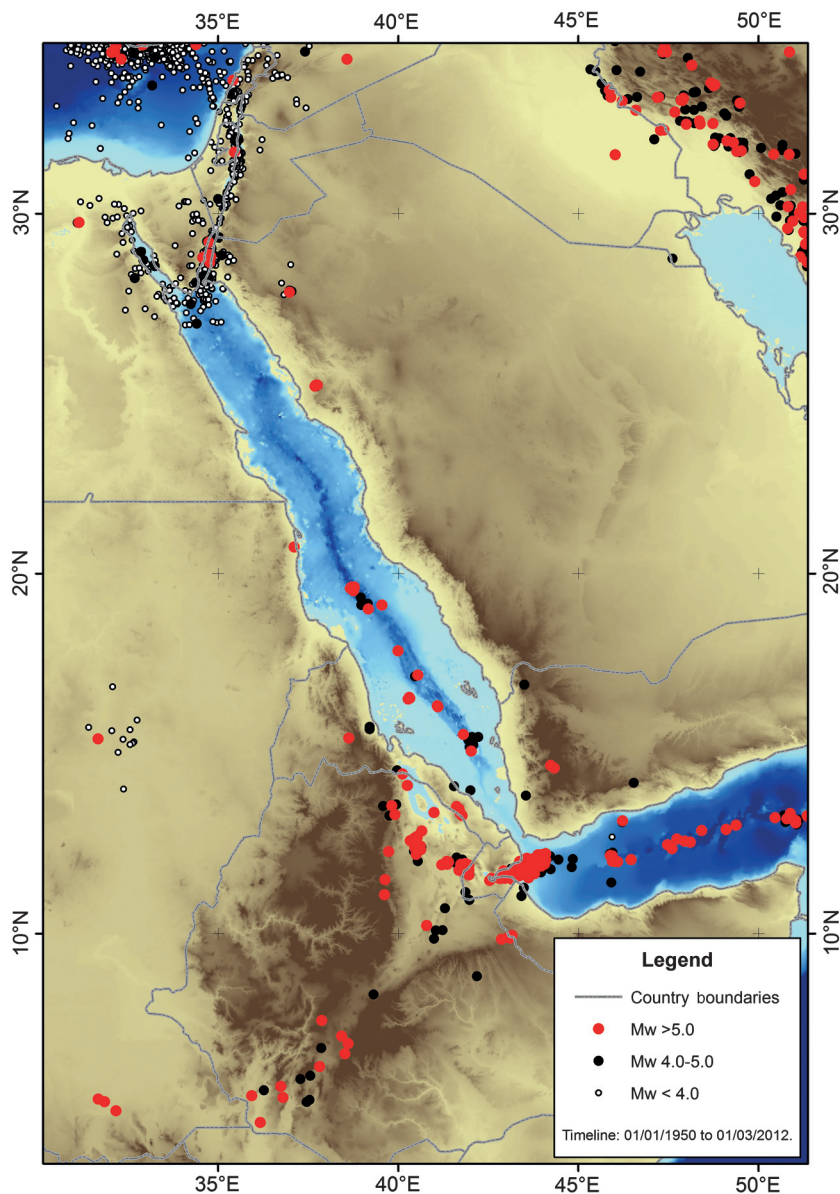


Figure 14. Seismicity of the Red Sea region 1950–2012 using moment magnitudes (Mw), overlain on terrain and bathymetry. These data are retrieved from the IISC Online Bulletin, (<http://www.isc.ac.uk>).

the gravity response, a significantly greater sediment depth is interpreted to the western side of the sea, apparently underlain by a series of faulted basement blocks. This increased sediment thickness is coincident with the area of shallowest Moho, offset westward from the center of the Red Sea. This association is consistent with an assumption of approximate isostatic balance.

Figure 15b shows the central Red Sea model along B-B'. The presence of a spreading center is inferred from the residual gravity map and approximately 80-km lateral extent of oceanic crust is required in the central part of the model to reproduce the gravity response. The model shows a nearly symmetric Moho bulge beneath this part of the Red Sea. In turn, the sediment is apparently of similar thickness either side of the sea, approaching a maximum thickness of 5–6 km east and west of the spreading center. To model the gravity successfully, we needed to remove the sedimentary layer

for approximately 8 km on either side of the spreading center. However, significant accumulations of sediment are required on the oceanic crust. This would be consistent with possible sediment sources from uplifted terrain on both margins.

Figure 15c shows the southern Red Sea model along C-C'. In a similar fashion to profile B-B', the gravity data indicate the presence of a spreading center. A slightly wider, approximately 85 km, lateral extent of oceanic crust is required in the central part of the model, consistent with the slightly earlier ocean opening in the south. Sediment is inferred to be absent (or very thin) approximately 16 km on either side of the central spreading ridge. However, thick accumulations of sediment are required on the flanks of the oceanic domain and, in particular, in the grabens on the stretched continental crust. This suggests a rich sediment supply from adjacent highlands from initial rifting onwards.

## DISCUSSION

We have shown that satellite gravity data can be an effective tool when interpreting the structure of the crust, upper mantle, and sedimentary basins for the Red Sea region. Integration with available land gravity data from surrounding areas is essential for modeling the Moho, as satellite (i.e., offshore) data alone provide an incomplete representation of the gravity anomalies from such depths. However, as the sedimentary basins barely extend onshore in this area, and must therefore be modeled based almost exclusively on satellite data, the land data are not required to be of high resolution. The available onshore data are adequate to control the long-wavelength gravity anomalies from Moho and upper mantle sources.

To interpret the deep geology (i.e., Moho depth and the variations in density contrast between the base of the crust and the upper mantle), the “regional” gravity anomaly associated with this boundary had to be separated from the

“residual” gravity anomaly related to sediments and other intracrustal features. Deeper sources tend to give broader gravity anomalies, and thus wavelength discrimination is generally a suitable approach for depth separation. In this area, the depth to the Moho varies greatly and there are geologic features with a range of widths, such that a simple single wavelength separation cannot be perfect. Moreover, the different gravity anomaly sources have similar trends and shapes and there will inevitably be some overlap of wavelengths. Despite this, we choose to continue with a simple wavelength filter separation method. The use of a simple filter has the advantage of being reasonably objective, thus avoiding the dangers of overly massaging the data to fit the desired outcome.

We tested a range of simple wavelength filters (100, 200, and 300 km — see Figure 7) and concluded that the 200-km filter provides an adequate separation over most of the area. The 100-km low-pass filter contains too much short wavelength signal, some of which, such as the subtle ridge along the Arabian coast, is incompatible with gravity anomalies from Moho depths. The 300-km low-

pass filter has very smooth slopes along the edges of the Red Sea, which are somewhat smoother than would be expected based on the seismic Moho depths. In some areas, such as the narrow rifts of the Gulfs of Suez and Aqaba, the 200-km filter is too broad to image the shallow Moho without aliasing, but in other areas such as the Arabian coast of the Red Sea, 200 km is just broad enough to avoid spurious anomalies in the regional field. In addition, the 200-km high-pass residual (Figure 8) shows continuous negative anomalies on each side of the Central and Southern Red Sea where elongate sedimentary basins are known to exist.

The Moho control depths from seismic studies provided a control on absolute Moho depths (as opposed to changes in Moho depth) and are also used for estimation of density contrasts at the Moho. This latter control is especially important in an area where the upper mantle and crustal densities are expected to vary significantly. The choice of a 50-km level for the effective base of the model, and hence, of the mantle density contrasts is somewhat arbitrary and unlikely to be completely true. The calculated density contrasts will

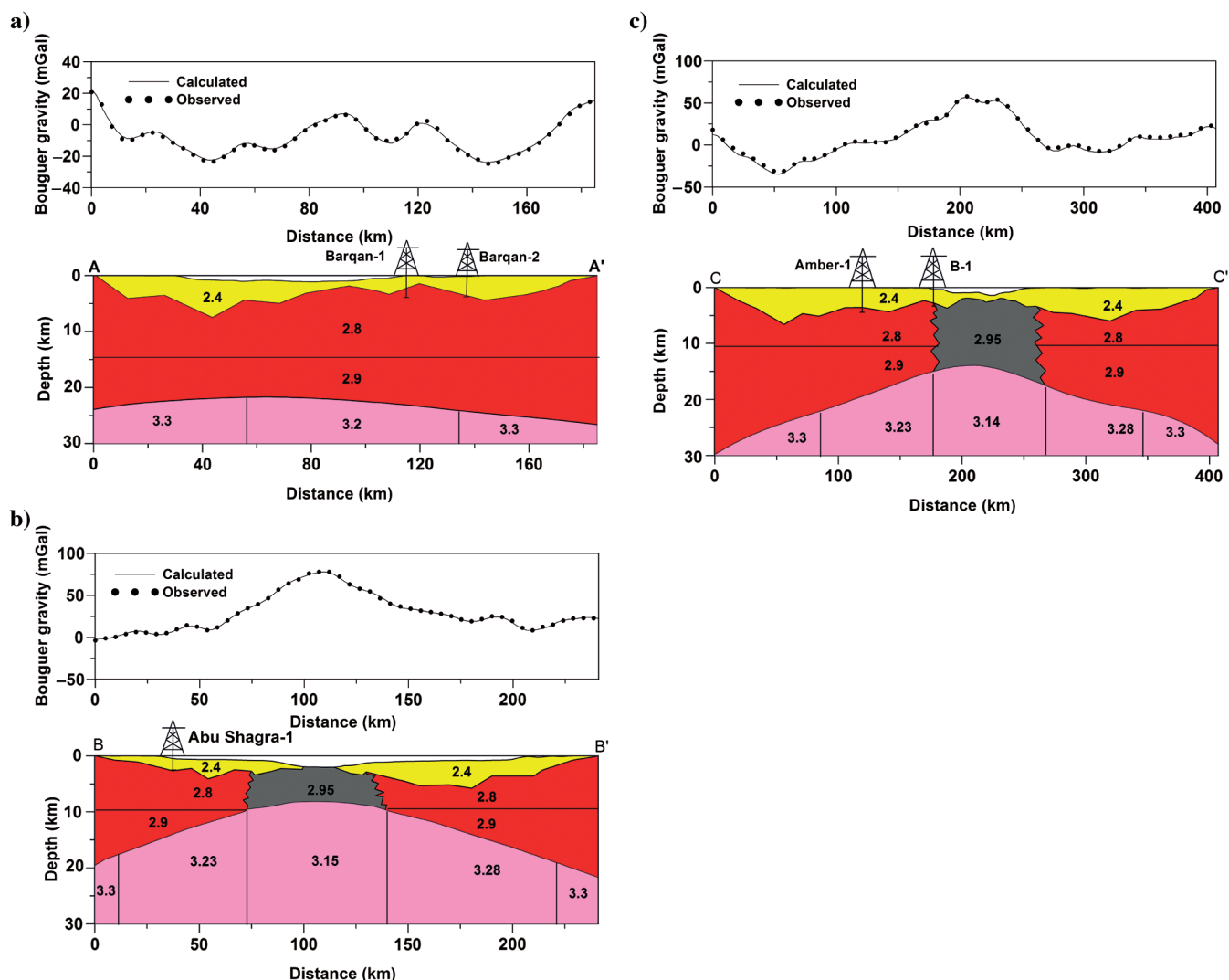


Figure 15. Two-dimensional gravity models of Bouguer anomaly data across the Red Sea. The three profiles (a) A-A', (b) B-B', and (c) C-C' are marked on Figure 12. In each model, the Moho depths and density values (in  $\text{g}/\text{cm}^3$ ) are taken from the earlier inversion (Figures 9 and 10). Basement wells (marked) provide further constraints.

consequently contain some errors. However, the effects on the calculated depths will be small as long as the density range is reasonable. The implied density variations in the uppermost mantle are within the range used by other authors (e.g., Makris et al., 1991). The control points are irregularly spaced and sparse on the African side, which increased the ambiguity between density variation and structure. However, our confidence in the regional interpretation is significantly enhanced by the correlation between interpreted density contrasts, upper mantle seismic velocities, and the expected temperature increase below an active rift.

Our interpretation indicated significant large-scale variation along the Red Sea. In the north, the rift and the basins above it are seen to be asymmetric, the crust is thick, and there is no prominent ridge. This suggests that this area is still in the continental rifting stage (e.g., Cochran and Martinez, 1988), where fault geometries, including a master fault on one side, as commonly seen in rift valleys, might be a typical configuration. Local magmatic intrusions into the crust, however, hint at the onset of ocean development. The central Red Sea shows a well-developed central ridge with largely symmetric crustal thinning and basin development. The crust is interpreted to be much thinner here and the upper-mantle density lower. We interpret all this to imply that this area is fully oceanic, although possibly quite young, and not a transition zone between continental rifting in the north and active seafloor spreading in the south, as proposed, for example, by Cochran and Martinez (1988). The southern Red Sea is interpreted to be similar to the central part with the exception of a narrower rift. This is thought to be the major spreading that has now migrated into the Afar Rift in the west (e.g., Bastow and Keir, 2011).

## CONCLUSION

We have used satellite gravity data, together with adjacent land gravity and seismic control, to map the Moho depth and model sedimentary thickness for the Red Sea region. Careful separation of the regional component of the gravity field is considered to be a key step in obtaining a gravity grid appropriate for inversion for Moho depth. In addition, independent constraint from published seismic data is considered to be crucial for the development of a viable density contrast model and to constrain the depth solution. Our results provide some significant insights into the crustal composition of the Red Sea, indicating that the Moho is shallowest along the central axis in the central Red Sea (<10 km), increasing to ~13 km to the south and ~20 km in the northern Red Sea. Our conclusion, based on the Moho inversion results, the modeled crustal densities, and the qualitative interpretation of the residual gravity component, is that the southern and central parts of the Red Sea are fully oceanic (albeit the central part is possibly very young), but the northern Red Sea is not yet oceanic. Based on this interpretation of the deep structure, profile modeling highlighted the presence of a system of large tilted fault blocks forming subbasins with a maximum thickness of approximately 6 km. With such an approach, uncertainties in the models will remain, reflecting input and constraint data limitations, imprecisions in density models and inherent smoothing in the inversion process. However, provided these limitations are understood, we conclude that the approach presented could be applied to aid the understanding of crustal composition and thickness over other continental margin areas where good data coverage and constraints exist.

## ACKNOWLEDGMENTS

We greatly appreciate the comments of Xiong Li on the manuscript. We are grateful for comments by Hassan H. Hassan and two anonymous reviewers that helped to improve the manuscript, as did extensive suggestions by associate editor, Richard Lane.

## REFERENCES

- Allan, T. D., 1970, Magnetic and gravity fields over the Red Sea: Philosophical Transactions of the Royal Society of London. Series A, Mathematical, Physical and Engineering Sciences, **267**, 153–180, doi: [10.1098/rsta.1970.0030](https://doi.org/10.1098/rsta.1970.0030).
- ArRajehi, A., S. McClusky, R. Reilinger, M. Daoud, A. Alchalbi, S. Ergintav, F. Gomez, J. Sholan, F. Bou-Rabee, G. Ogubazghi, B. Haileab, S. Fisseha, L. Asfaw, S. Mahmoud, A. Rayan, R. Bendik, and L. Kogan, 2010, Geodetic constraints on present-day motion of the Arabian Plate: Implications for Red Sea and Gulf of Aden rifting: Tectonics, **29**, TC3011, doi: [10.1029/2009TC002482](https://doi.org/10.1029/2009TC002482).
- Avedik, F., L. Geli, J. M. Gaulier, and J. P. Le Format, 1988, Results from three refraction profiles in the Northern Red Sea (above 25°N) recorded with an ocean bottom vertical seismic array: Tectonophysics, **153**, 89–101, doi: [10.1016/0040-1951\(88\)90008-X](https://doi.org/10.1016/0040-1951(88)90008-X).
- Bastow, I. D., and D. Keir, 2011, The protracted development of the continent-ocean transition in afar: Nature Geoscience, **4**, 248–250, doi: [10.1038/ngeo1095](https://doi.org/10.1038/ngeo1095).
- Beydoun, Z. R., and A. H. Sikander, 1992, The Red Sea-Gulf of Aden: Re-assessment of hydrocarbon potential: Marine and Petroleum Geology, **9**, 474–485, doi: [10.1016/0264-8172\(92\)90060-R](https://doi.org/10.1016/0264-8172(92)90060-R).
- Bosworth, B., and K. Burke, 2005, Evolution of the Red Sea as Gulf of Aden Rift System: Gulf Coast Association Petroleum Societies 25th Annual Bob Perkins Research Conference: Petroleum systems of divergent continental margin basins, 342–372.
- Chappell, A. R., and N. J. Kusznir, 2008, Three-dimensional gravity inversion for Moho depth at rifted continental margins incorporating a lithosphere thermal gravity anomaly correction: Geophysical Journal International.
- Cochran, J. R., and G. D. Karner, 2007, Constraints on the deformation and rupturing of continental lithosphere of the Red Sea: The transition from rifting to drifting: Geological Society of London, Special Publication 282, 265–289.
- Cochran, J., and F. Martinez, 1988, Evidence from the northern Red Sea on the transition from continental to oceanic rifting: Tectonophysics, **153**, 25–53, doi: [10.1016/0040-1951\(88\)90006-6](https://doi.org/10.1016/0040-1951(88)90006-6).
- Cochran, J., F. Martinez, M. S. Steckler, and M. A. Hobart, 1986, Conrad Deep: A northern Red Sea deep. Origin and implication for continental rifting: Earth and Planetary Science Letters, **78**, 18–32, doi: [10.1016/0012-821X\(86\)90169-X](https://doi.org/10.1016/0012-821X(86)90169-X).
- Egloff, F., R. Rihm, J. Markris, Y. A. Izzeldin, M. Bobsien, K. Meier, P. Junge, T. Noman, and W. Warsi, 1991, Contrasting structural styles of the eastern and western margins of the southern Red Sea: The 1988 SONNE experiment: Tectonophysics, **198**, 329–353, doi: [10.1016/0040-1951\(91\)90159-P](https://doi.org/10.1016/0040-1951(91)90159-P).
- Ehrhardt, A., C. Hübscher, and D. Gajewski, 2005, Conrad Deep, northern Red Sea: Development of an early stage ocean deep within the axial depression: Tectonophysics, **411**, 19–40, doi: [10.1016/j.tecto.2005.08.011](https://doi.org/10.1016/j.tecto.2005.08.011).
- Fairhead, J. D., and R. W. Girdler, 1970, The seismicity of the Red Sea, Gulf of Aden and Afar triangle: Philosophical Transactions of the Royal Society of London. Series A, Mathematical, Physical and Engineering Sciences, **267**, 49–74, doi: [10.1098/rsta.1970.0023](https://doi.org/10.1098/rsta.1970.0023).
- Fairhead, J. D., S. E. Williams, K. M. U. Fletcher, C. M. Green, and K. Vincent, 2009, Trident — A new satellite gravity model for the oceans: 71st Annual Conference and Exhibition, EAGE.
- Gaulier, J. M., X. LePichon, N. Lyberis, F. Avedik, L. Geli, I. Moretti, A. Deschamps, and H. Salah, 1988, Seismic study of the crust of the northern Red Sea and Gulf of Suez: Tectonophysics, **153**, 55–88, doi: [10.1016/0040-1951\(88\)90007-8](https://doi.org/10.1016/0040-1951(88)90007-8).
- Ghebreab, W., 1998, Tectonics of the Red Sea region reassessed: Earth-Science Reviews, **45**, 1–44, doi: [10.1016/S0012-8252\(98\)00036-1](https://doi.org/10.1016/S0012-8252(98)00036-1).
- Green, C. M., and J. D. Fairhead, 1996, New 5' × 5' digital gravity and terrain models of the earth, in R. H. Rapp, A. A. Casenave, and R. S. Nerem, eds., Global gravity field and its temporal variations: IAG Symposia, 116, Springer-Verlag.
- Hansen, S. E., A. J. Rodgers, S. Y. Schwartz, and M. S. Abdullah Al-Amri, 2007, Imaging ruptured lithosphere beneath the Red Sea and Arabian Peninsula: Earth and Planetary Science Letters, **259**, 256–265, doi: [10.1016/j.epsl.2007.04.035](https://doi.org/10.1016/j.epsl.2007.04.035).
- Izzeldin, A. Y., 1987, Seismic, gravity and magnetic surveys in the central part of the Red Sea: Their interpretation and implications for the structure

- and evolution of the Red Sea: *Tectonophysics*, **143**, 269–306, doi: [10.1016/0040-1951\(87\)90214-9](https://doi.org/10.1016/0040-1951(87)90214-9).
- Makris, J., C. H. Henke, F. Egloff, and T. Akamaluk, 1991, The gravity field of the Red Sea and East Africa: *Tectonophysics*, **198**, 369–381, doi: [10.1016/0040-1951\(91\)90161-K](https://doi.org/10.1016/0040-1951(91)90161-K).
- Maus, S., U. Barckhausen, H. Berkenbosch, N. Bournas, J. Brozena, V. Childers, F. Dostaler, J. D. Fairhead, C. Finn, R. R. B. von Frese, C. Gaina, S. Golynsky, R. Kucks, H. Lühr, P. Milligan, S. Mogren, R. D. Müller, O. Olesen, M. Pilkington, R. Saltus, B. Schreckenberger, E. Thébaud, and F. Caratori Tontini, 2009, EMAG2: A 2-arc min resolution earth magnetic anomaly grid compiled from satellite, airborne, and marine magnetic measurements: *Geochemistry, Geophysics, Geosystems*, **10**, Q08005, doi: [10.1029/2009GC002471](https://doi.org/10.1029/2009GC002471).
- McKenzie, D. P., 1978, Some remarks on the development of sedimentary basins: *Earth and Planetary Science Letters*, **40**, 25–32, doi: [10.1016/0012-821X\(78\)90071-7](https://doi.org/10.1016/0012-821X(78)90071-7).
- Parker, R., 1973, The rapid calculation of potential anomalies: *Geophysical Journal of the Royal Astronomical Society*, **31**, 447–455, doi: [10.1111/j.1365-246X.1973.tb06513.x](https://doi.org/10.1111/j.1365-246X.1973.tb06513.x).
- Pavlis, N. K., S. A. Holmes, S. C. Kenyon, and J. K. Factor, 2012, The development and evaluation of the earth gravitational model 2008 (EGM2008): *Journal of Geophysical Research*, **117**, B04406, doi: [10.1029/2011JB008916](https://doi.org/10.1029/2011JB008916).
- Phillips, J. D., 1970, Magnetic anomalies in the Red Sea: *Philosophical Transactions of the Royal Society of London. Series A. Mathematical, Physical and Engineering Sciences*, **267**, 205–217, doi: [10.1098/rsta.1970.0033](https://doi.org/10.1098/rsta.1970.0033).
- Prodehl, C., 1985, Interpretation of a seismic refraction profile across the Arabian Shield in western Saudi Arabia: *Tectonophysics*, **111**, 247–282, doi: [10.1016/0040-1951\(85\)90288-4](https://doi.org/10.1016/0040-1951(85)90288-4).
- Prodehl, C., K. Fuchs, and J. Mechie, 1997, Seismic-refraction studies of the Afro-Arabian rift system — A brief review: *Tectonophysics*, **278**, 1–13, doi: [10.1016/S0040-1951\(97\)00091-7](https://doi.org/10.1016/S0040-1951(97)00091-7).
- Prodehl, C., and J. Mechie, 1991, Crustal thinning in relationship to the evolution of the Afro-Arabian rift system: A review of seismic-refraction data: *Tectonophysics*, **198**, 311–327, doi: [10.1016/0040-1951\(91\)90158-O](https://doi.org/10.1016/0040-1951(91)90158-O).
- Prutkin, I., and A. Saleh, 2009, Gravity and magnetic data inversion for 3D topography of the Moho discontinuity in the northern Red Sea area, Egypt: *Journal of Geodynamics*, **47**, 237–245, doi: [10.1016/j.jog.2008.12.001](https://doi.org/10.1016/j.jog.2008.12.001).
- Richter, H., J. Makris, and R. Rihm, 1991, Geophysical observations offshore Saudi Arabia: seismic and magnetic measurements: *Tectonophysics*, **198**, 297–310, doi: [10.1016/0040-1951\(91\)90157-N](https://doi.org/10.1016/0040-1951(91)90157-N).
- Roeser, H. A., 1975, A detailed magnetic survey of the southern Red Sea: *Geologisches Jahrbuch*, **13**, 131–153.
- Seber, D., E. Sandvol, C. Sandvol, C. Brindisi, and M. Barazangi, 2001, Crustal model for the Middle East and North Africa region: Implications for the isostatic compensation mechanism: *Geophysical Journal International*, **147**, 630–638, doi: [10.1046/j.0956-540x.2001.01572.x](https://doi.org/10.1046/j.0956-540x.2001.01572.x).